NUMERICAL SIMULATION OF GEOPHYSICAL TURBULENCE

Piotr K Smolarkiewicz*
*National Center for Atmospheric Research, Boulder, Colorado, U.S.A.

Figure 1: Geophysical turbulence; scales $\mathcal{O}(10^7)$, $\mathcal{O}(10^4)$, and $\mathcal{O}(10^{-2})$ m.

• Geophysical turbulence embodies phenomena uncommon in engineering applications, such as breaking of internal inertia-gravity waves (viz. *localization*) and spans an enormous range of scales; e.g., $\kappa \sim \mathcal{O}(10^{20})$, for the Earth atmosphere.

Geophysical turbulence is intermittent in nature. This dictates three useful (for research) simulation strategies:

- direct numerical simulation (DNS), with all relevant scales of motion resolved, thus admitting variety of numerical methods;
- large-eddy simulation (LES), with all relevant subgrid scales parameterized, thus preferring higher-order methods;
- implicit large-eddy simulation (ILES) — alias monotonically-integrated large-eddy-simulation (MILES), or implicit turbulence modeling — with a bohemian attitude toward subgrid scales and available only with selected numerical methods.

• ILES a “do-nothing” approach that relies on nonoscillatory (physically-motivated) numerics that “adapts” itself to the flow in the course of a simulation $\Leftrightarrow$ in progress and controversial, yet effective and relatively simple; i.e., practical.

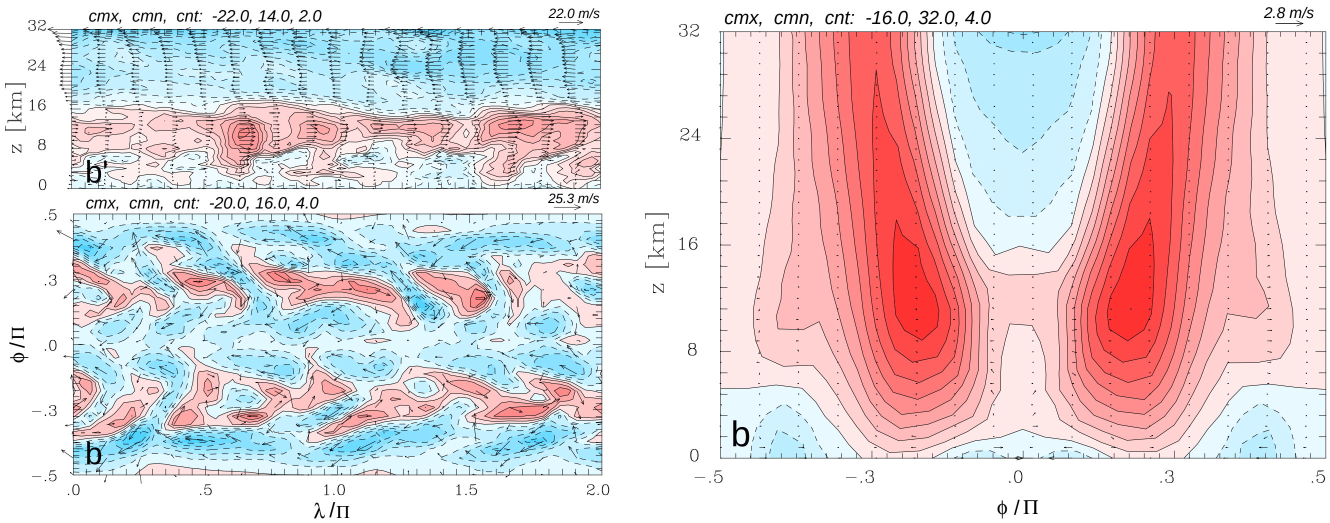

Figure 2: The idealized Held-Suarez climate problem (*BAMS* 1994); instantaneous solution after 3 years of simulation (left), and zonally averaged 3-year means (right) (Sm. et al. *JAS* 2001).

RE: ILES Justification

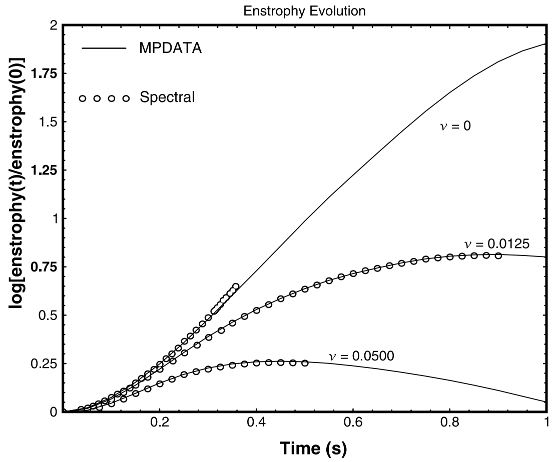

Figure 3: 256^3 DNS/ILES of transient decaying turbulence; Margolin et al. *J. Fluid Eng.* 2002.

time	1.00	1.25	1.50	1.75	2.00
$-15 < u_x^3 > \delta x^2/(4\varepsilon)$	0.785	0.933	1.028	1.054	1.019

Table 1: Verification of "4/5" Kolmogorov's law $\langle(\delta v_{\,||}(\mathbf{r},\mathbf{l}))^3\rangle = -\frac{4}{5}\varepsilon l \quad \Rightarrow \varepsilon \sim v_o^3/l_o$; $\delta v_{||}(\mathbf{r},\mathbf{l}) := [\mathbf{v}(\mathbf{r}+\mathbf{l}) - \mathbf{v}(\mathbf{r})]\cdot(\mathbf{l}/l),\ \ v_o := \sqrt{\langle \mathbf{v}(\mathbf{r}+\mathbf{l}_o)\cdot\mathbf{v}(\mathbf{r})\rangle}$ — Frisch 1995.

RE: More ILES Justification

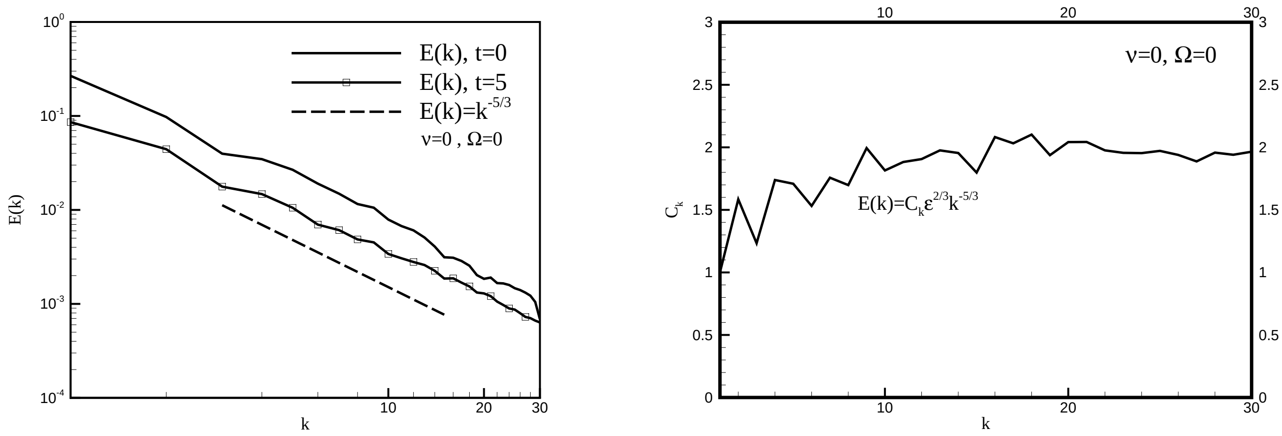

Figure 4: 64^3 ILES of decaying turbulence, Domaradzki et al. *Phys. Fluids* 2003. Energy spectra and Kolmogorov function $C_K(k) = \varepsilon^{-2/3} k^{5/3} E(k)$ dla $\nu = 0.0$ $\Leftrightarrow$ $\langle (\delta v_{\|}(l))^2 \rangle \sim l^{2/3}$

• LES with physically-motivated SGS models $\Leftrightarrow$ theoretically not universal enough, and practically much more complicated than ILES, but effective for shear-driven boundary layer flows.

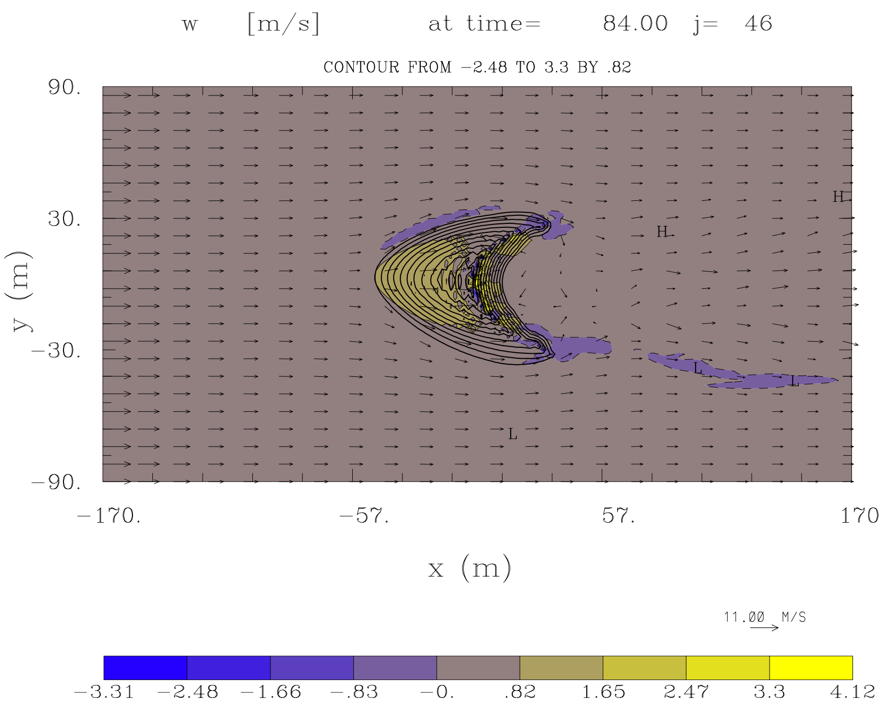

Figure 5: LES of PBL past a rapidly evolving sand dune; Ortiz & Sm., *IJNMF* 2005

Simulations of boundary layer flows past sand dunes — $340\times180\times 40\ \mathrm{m}^3$ domain covered with $\delta x = \delta y = 2\mathrm{m},\ \delta z = 1\ \mathrm{m}$ — depend on explicit SGS model (here TKE), because the saltation physics that controls dune evolution depends crucially on the boundary stress.

• DNS $\Leftrightarrow$ TRUE, although limited to low Reynolds number flows, a useful complement of laboratory experiments.

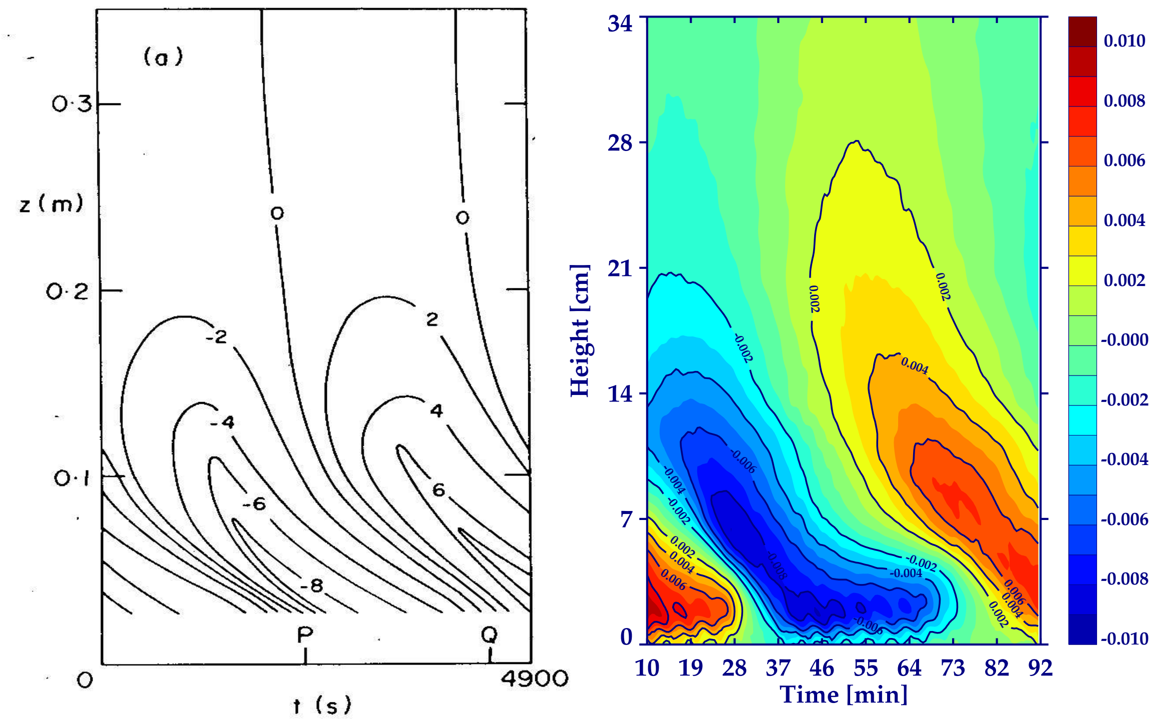

Figure 6: Time-height cross-section of the observed zonal-mean zonal fbw velocity component (plate (a), adapted from Fig.10 in Plumb & McEwan (1978), contour lines are in mms^{-1}), compared to the result of the 3D numerical simulation at $y = L_y/2$ (plate (b), contour lines are in ms^{-1}). According to Plumb & McEwan (1978), the lowest 2 cm in plate (a) could not be observed due to restrictions of the viewing window; Nils Wedi, Ph.D thesis, $+$.

- With mesh adaptivity for simulating complex geophysical flows in mind, we have developed a generalized mathematical framework for the implementation of deformable coordinates in a generic Eulerian/ semi-Lagrangian format of nonoscillatory-forward-in-time (NFT) schemes.

- There is more involved than a mere application of well-known mathematical theories. Technical apparatus of the Riemannian Geometry must be applied judiciously, in order to arrive at an effective numerical model.

Anelastic Model: Analytic Formulation

Prusa & Sm., *JCP* 2003; Wedi & Sm., *JCP* 2004

- *diffeomorphic* mapping

$$(\bar{t}, \bar{x}, \bar{y}, \bar{z}) \equiv (\ t,\ E(t,x,y),\ D(t,x,y),\ C(t,x,y,z)\ )\ , \qquad (1)$$

(t,x,y,z) does not have to be Cartesian!

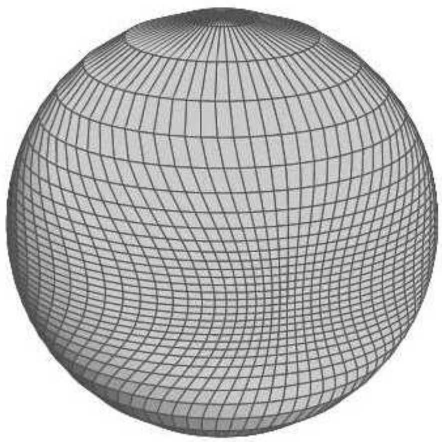

Figure 7: Continuous global mesh transformation, an example

- Anelastic system of Lipps & Hemler (*JAS*, 1982)

$$\frac{\partial(\rho^* \overline{v^s}^k)}{\partial \overline{x}^k} = 0 \ . \tag{2}$$

$$\frac{dv^j}{d\overline{t}} = - \widetilde{G}^k_j \frac{\partial \pi'}{\partial \overline{x}^k} + g\frac{\theta'}{\theta_b}\delta_3{}^j + \mathcal{F}^j + \mathcal{V}^j \ , \tag{3}$$

$$\frac{d\theta'}{d\overline{t}} = -\overline{v^s}^k \frac{\partial \theta_e}{\partial \overline{x}^k} + \mathcal{H} \ , \tag{4}$$

$$\overline{v^s}^k := \overline{v^*}^k - \frac{\partial \overline{x}^k}{\partial t} \quad ; \quad \overline{v^s}^j = \widetilde{G}^j_k v^k \ . \tag{5}$$

$$\rho^* := \rho_b \overline{G} \ \ ; d/d\overline{t} = \partial/\partial\overline{t} + \overline{v^*}^k(\partial/\partial\overline{x}^k) \ \ ; \ \ \overline{v^*}^k := d\overline{x}^k/d\overline{t} := \dot{\overline{x}}^k$$

$$\widetilde{G}^k_j := \sqrt{g^{jj}}(\partial\overline{x}^k/\partial x^j) \ \ \Leftarrow \ \ ds^2 = g_{pq}dx^p dx^q \ , \ \ g_{pk}g^{kq} \equiv \delta^q_p$$

RE: Technical apparatus must be applied judiciously...

- VORTICITY (simple substantiation compared to STRESS)

$$\overline{\omega}^{*}{}_{jk} = \overline{v}^{*}{}_{k,j} - \overline{v}^{*}{}_{j,k} \;\; \Rightarrow \;\; \omega^{q} = \varepsilon_{qjk}\sqrt{g^{kk}}\; \widetilde{G}^{p}_{j}\frac{\partial\sqrt{g_{kk}}v^{k}}{\partial\overline{x}^{p}} \; ; \qquad (6)$$

in any system $\overline{v}^{*}{}_{k} = \overline{g}_{jk}\,\overline{v}^{*j}$, so in the physical space $v^{*}{}_{j} = \sqrt{g_{jj}}v^{j}$.

$$\nabla \bullet \boldsymbol{\omega} = \nabla \bullet \nabla \times \mathbf{v} \equiv 0 \;\; \Rightarrow$$

$$\frac{1}{\overline{\overline{G}}}\frac{\partial}{\partial\overline{x}^{p}}(\overline{G}\overline{\omega^{sp}}) \equiv 0 \;\; , \;\; \overline{\omega^{sp}} := \widetilde{G}^{q}_{p}\omega^{q} \; . \qquad (7)$$

Note the connection with the solenoidal velocity in (5)!

• Example: flapping membranes (Wedi & Sm., *JCP*, 2004)

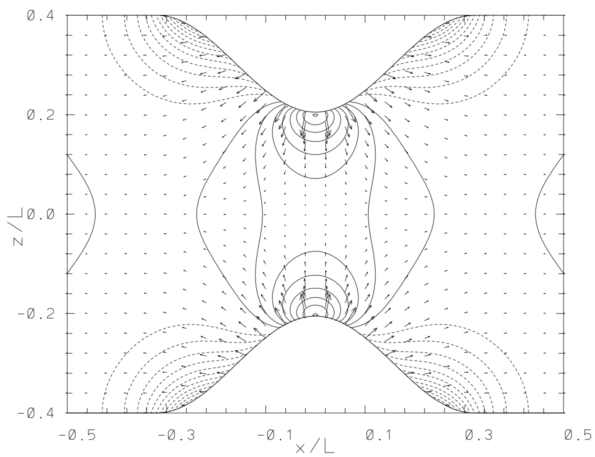

Figure 8: Potential fbw simulation past 3D undulating boundaries

Table 2: Vorticity errors in a potential fbw simulation

fi eld	Max |.|	Average	Standard deviation
$\Delta t\omega^1$	$6.99{\cdot}10^{-2}$	$-4.87{\cdot}10^{-18}$	$1.90{\cdot}10^{-3}$
$\Delta t\omega^2$	$6.98{\cdot}10^{-2}$	$-3.19{\cdot}10^{-17}$	$1.90{\cdot}10^{-3}$
$\Delta t\omega^3$	$7.62{\cdot}10^{-3}$	$2.20{\cdot}10^{-18}$	$1.71{\cdot}10^{-4}$
$\Delta t\Delta x\nabla \bullet \boldsymbol{\omega}^s$	$3.73{\cdot}10^{-3}$	$2.12{\cdot}10^{-17}$	$4.81{\cdot}10^{-5}$

• MOMENTUM DISSIPATION

$$\overline{\epsilon}^*{}_{jk} \equiv \frac{1}{2}\left(\overline{v}^*{}_{k,j} + \overline{v}^*{}_{j,k}\right) \tag{8}$$

Strain rate, the symmetric complement of the *rotation* (viz. $0.5\overline{\omega}^*{}_{jk}$ in Eq. (6)) to the gradient of the covariant velocity, the *objective* form.

Provision of the dissipative term $\mathcal{V} \sim$ **Div** $\bullet\, \boldsymbol{\tau}$ in momentum equation (3) requires a number of conversions:

$$\epsilon^*_{jk} \equiv \frac{1}{2}\left(\sqrt{g_{kk}}\,\widetilde{G}^p_k \frac{\partial\sqrt{g_{jj}}v^j}{\partial\overline{x}^p} + \sqrt{g_{jj}}\,\widetilde{G}^q_j \frac{\partial\sqrt{g_{kk}}v^k}{\partial\overline{x}^q}\right) - \sqrt{g_{mm}}\left\{\begin{matrix} m \\ j \;\; k \end{matrix}\right\} v^m \,.$$

$$\rho_b \tau^{*j}_{\;\;k} := 2\mu\epsilon^{*j}_{\;\;k} + \lambda v^{*m}_{\;\;,m}\delta^j_k) \Rightarrow \mathcal{V}^j \equiv \sqrt{g_{jj}}\rho_b^{-1}(\rho_b\tau^{*jk})_{,k}$$

$$\mathcal{V}^j = \frac{1}{\rho^*}\frac{\partial}{\partial\overline{x}^p}\left(\rho^*\widetilde{G}^p_k\sqrt{g_{jj}g_{kk}}\tau^{*jk}\right) - \tau^{*jk}\frac{\partial\sqrt{g_{jj}}}{\partial x^k} + \sqrt{g_{jj}}\left\{\begin{matrix} j \\ l \;\; m \end{matrix}\right\}\tau^{*lm} \,;$$

$$\tau^{*jk} = 2\nu g^{jj}g^{kk}\epsilon^*{}_{jk} + \kappa g^{jk}v^{*m}_{\;\;,m} \,;\;\; \nu := \mu/\rho \,,\; \kappa := \lambda/\rho \,. \tag{9}$$

• TENSOR IDENTITIES

$$\frac{\mathcal{D}\phi}{\mathcal{D}t} \equiv \frac{\partial \phi}{\partial x^q} v^q \equiv \frac{\partial \phi}{\partial \overline{x}^r} \frac{\partial \overline{x}^r}{\partial x^q} v^q \equiv \frac{\partial \phi}{\partial \overline{x}^r} \overline{v}^r =: \frac{\mathcal{D}\phi}{\mathcal{D}\overline{t}} \ . \tag{10}$$

$$\frac{D\overline{v}^{*j}}{D\overline{t}} := \overline{v}^{*j}_{,m} \overline{v}^{*m} \equiv \frac{d\overline{v}^{*j}}{d\overline{t}} + \overline{\begin{Bmatrix} j \\ i \ \ m \end{Bmatrix}} \overline{v}^{*i} \overline{v}^{*m} \ . \tag{11}$$

$$\delta^r_s \equiv \frac{\partial \overline{x}^r}{\partial x^q} \frac{\partial x^q}{\partial \overline{x}^s} \ . \tag{12}$$

$$\frac{G}{\overline{G}} \frac{\partial}{\partial \overline{x}^r} \left(\frac{\overline{G}}{G} \frac{\partial \overline{x}^r}{\partial x^s} \right) \equiv 0 \ . \tag{13}$$

Sm.. & Prusa, in *Turbulent Flow Computation*, Kluver, 2002

• Each prognostic equation can be written as either *Lagrangian* evolution equation or *Eulerian* conservation law:

$$\frac{d\psi}{d\bar{t}} = R \ , \quad \frac{\partial \rho^* \psi}{\partial \bar{t}} + \overline{\nabla} \bullet (\rho^* \overline{\mathbf{v}}^* \psi) = \rho^* R \ . \tag{14}$$

$\psi \equiv v^j$ or θ', and R the associated rhs, $\overline{\nabla}\bullet := (\partial/\partial\bar{x},\ \partial/\partial\bar{y},\ \partial/\partial\bar{z})\bullet$.

• Either form is approximated to $\mathcal{O}(\delta t^2, \delta x^2)$

$$\psi_{\mathbf{i}}^{n+1} = LE_{\mathbf{i}}(\psi^n + 0.5\Delta t R^n) + 0.5\Delta t R_{\mathbf{i}}^{n+1} \ ; \tag{15}$$

where $\psi_{\mathbf{i}}^{n+1}$ is the solution sought at the grid point $(\bar{t}^{n+1}, \overline{\mathbf{x}}_{\mathbf{i}})$, LE denotes a two-time-level either advective semi-Lagrangian or flux-form Eulerian NFT transport operator (Sm. & Pudykiewicz, *JAS*, 1992; Sm. & Margolin, *MWR* 1993).

• (15) represents an algebraic system implicit for all $\psi \Rightarrow$ BVP(π) .

• Example (complete): LES of a moist mesoscale valley flow

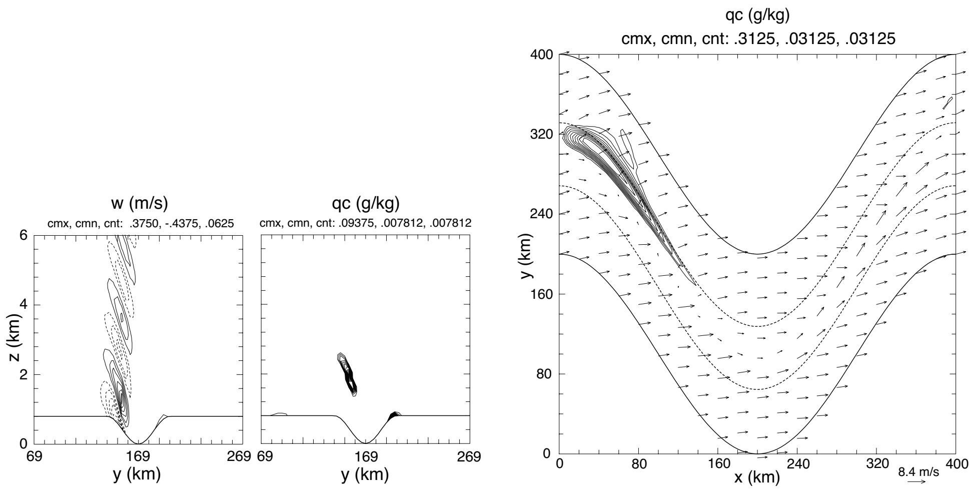

Figure 9: Vertical velocity (outer left panel) and cloud water mixing ratio (inner left panel) in the yz cross section at $x = 120$ km and cloud-water mixing ratio at bottom surface of the model (right panel); Sm. & Prusa, *IJNMF* 2005.

Remarks

• Synergetic interaction between (i) rules of continuous mapping, (ii) strengths of nonoscillatory forward-in-time (NFT) numerical schemes, and (iii) virtues of the anelastic formulation of the governing equations of motion facilitates designing a robust multi-scale research model for geophysical turbulence.

RE (i): e.g., benefits of satisfying the tensor identities at finite-difference level

RE (ii): e.g., benefits of NFT numerical methods for computations on dynamically deforming grids (nested grids)

RE (iii): e.g., benefits of the elliptic BVP rigor imposed by anelastic systems for elastic and compressible clones

- ... a robust multi-scale research model for geophysical turbulence

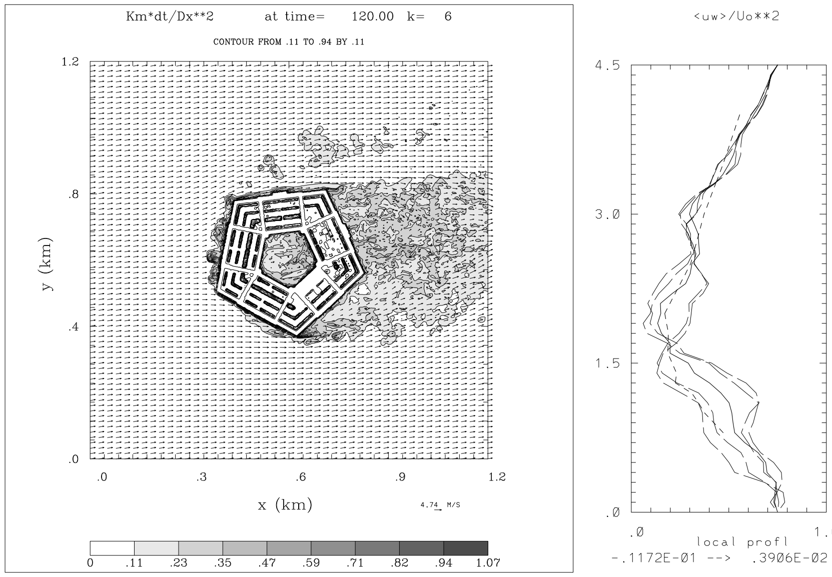

Figure 10: Urban PBL; $\sqrt{TKE}$ contours in xy cross section at z=10 m (left), and normalized $< u'w' >$ profiles at a location in the wake (right).